

# Generalized Coherent Photogalvanic Effect in Coherently Seeded Waveguides

Ozan Yakar, Edgars Nitiss, Jianqi Hu, and Camille-Sophie Brès\*

The coherent photogalvanic effect leads to the generation of a current under the absorption interference of coherent beams and allows for the inscription of space-charge gratings leading to a second-order susceptibility ( $\chi^{(2)}$ ). The inscribed grating automatically results in quasi-phase-matching between the interfering beams. Theoretical and experimental studies, considering the degenerate case of second-harmonic generation, show significant conversion efficiency enhancements. However, the link between the theory and experiment is not fully established such that general guidelines and achievable conversion efficiency for a given material platform are still unclear. In this work, the phenomenological model of coherent photogalvanic effect in optical waveguides is theoretically analyzed. This model predicts the existence of non-degenerate sum-frequency generation quasi-phase-matching gratings, which is confirmed experimentally for the first time. Furthermore, the time dynamics of the space-charge grating inscription in coherent photogalvanic process is formulated. Based on the developed theoretical equations, the material parameters governing the process for stoichiometric silicon nitride are extracted. The results obtained provide a basis to compare the performances and potentials of different platforms. This work not only supplements the theory of coherent photogalvanic effect, but also enables us to identify critical parameters and limiting factors for the inscription of  $\chi^{(2)}$  gratings.


photogalvanic effect (PGE), have been utilized to induce effective second-order nonlinear susceptibility ( $\chi^{(2)}$ ) in glasses with a technique called all-optical poling (AOP). During AOP,  $\chi^{(2)}$  susceptibility results from the product of generated DC field, caused by coherent currents, and third-order susceptibility  $\chi^{(3)}$  of the medium. In addition, the phase dependence of coherent currents allows the inscription of periodically sign alternating  $\chi^{(2)}$  gratings by coupling strong fundamental harmonic pump to the waveguide. The latter leads to quasi-phase-matching (QPM) for momentum conservation amongst the involving photons and efficient energy conversion in nonlinear optical interactions. Such automatic QPM was intensely studied, predominantly for second-harmonic generation (SHG), both theoretically<sup>[9–13]</sup> as well as experimentally<sup>[14–19]</sup> in optical fibers more than two decades ago. However, the link between theory and experiment, as well as the influence of the material parameters remained mostly unexplored.

In recent years, AOP was also demonstrated in integrated photonics, both in waveguides<sup>[20–22]</sup> and microring resonators,<sup>[23,24]</sup> and photoinduced second-order nonlinearity regained significant attention. In all these earlier works spontaneous growth of SHG in the stoichiometric silicon nitride ( $\text{Si}_3\text{N}_4$ ) waveguide devices was observed in the presence of strong pump. Earlier demonstrations have also revealed the shapes of charge separated gratings that support the degenerate three-wave mixing process in the integrated photonics platform. The latter offers improved modal confinement allowing high intensities under reduced powers compared to optical fibers and increased flexibility for dispersion engineering. Particularly,  $\text{Si}_3\text{N}_4$  with its large transparency window, low losses, high third-order susceptibility ( $\chi^{(3)}$ ), high refractive index, and mature nanofabrication process is very appealing. It is exploited for several linear<sup>[25]</sup> and nonlinear applications, such as four-wave mixing,<sup>[26,27]</sup> third-harmonic generation (THG),<sup>[28]</sup> supercontinuum,<sup>[29]</sup> and Kerr comb<sup>[30]</sup> generation using  $\chi^{(3)}$  nonlinearity. AOP now allows to add  $\chi^{(2)}$  processes, such as SHG, difference-frequency generation,<sup>[31]</sup> and spontaneous parametric down-conversion,<sup>[32]</sup> to the already impressive nonlinear toolbox of  $\text{Si}_3\text{N}_4$ . Recently, there have been several qualitative attempts to explain the time dynamics of AOP, which exhibits growth and saturation, and its dependence

## 1. Introduction

All-optical control of currents in centrosymmetric media has been a widely pursued objective for over half a century.<sup>[1]</sup> Caused by the quantum interference of multiphoton absorption, coherent currents facilitate several physical and chemical processes.<sup>[1–10]</sup> Coherent currents, resulting from the coherent

O. Yakar, E. Nitiss, J. Hu, C.-S. Brès  
Photonic Systems Laboratory (PHOSL)  
École Polytechnique Fédérale de Lausanne (EPFL)  
Lausanne CH-1015, Switzerland  
E-mail: camille.bres@epfl.ch

 The ORCID identification number(s) for the author(s) of this article can be found under <https://doi.org/10.1002/lpor.202200294>

© 2022 The Authors. Laser & Photonics Reviews published by Wiley-VCH GmbH. This is an open access article under the terms of the Creative Commons Attribution-NonCommercial-NoDerivs License, which permits use and distribution in any medium, provided the original work is properly cited, the use is non-commercial and no modifications or adaptations are made.

DOI: 10.1002/lpor.202200294

on waveguide dimensions.<sup>[21,22,33]</sup> However, a quantitative assessment is still lacking with unknown material constants, while the seeding mechanism of the process remains elusive.<sup>[13,34–38]</sup> With two-photon microscopy (TPM) imaging, charge gratings have been observed,<sup>[21]</sup> providing crucial information in terms of interacting modes. However, the length of the grating always remained shorter than half of the waveguide length<sup>[21,22]</sup> suggesting that the light conversion efficiency could be further increased. Overall, the origin and physical limitations of AOP remain unclear. A possible approach for quantitative analysis, and therefore a mean to optimize efficiencies, is to use a seeded approach where a coherent second-harmonic (SH) is externally coupled together with its pump. With such a seeded approach, the required time and powers for AOP were significantly reduced in fibers,<sup>[18]</sup> while the efficiencies could be increased. As such, AOP is initiated in a more efficient and controlled fashion.

In this work, based on the model initially proposed by Dianov et al.,<sup>[13]</sup> we develop a general phenomenological model that predicts the existence of non-degenerate sum-frequency generation (SFG) QPM gratings and set the basis for explaining the dynamics of AOP in waveguides. Our model is experimentally validated with the first observation of SFG QPM gratings initiated by the coherent interaction of a pump and its SH in a  $\text{Si}_3\text{N}_4$  waveguide. In addition, we formulate the time dynamics of the SHG process enabled by coherent PGE. The dynamic model serves as a basis for the extraction of material parameters critical in the inscription of the  $\chi^{(2)}$  gratings, which now provides a mean to benchmark the performances of different material platforms. In our case, we apply this approach to  $\text{Si}_3\text{N}_4$  through a series of experiments, relying on a seeded AOP scheme. Finally, we show that such information is essential and can be used in establishing the net conversion efficiency limitation and energy requirements of the AOP process, thus setting an important building block in the optimization of such devices. The remainder of the paper is organized as follows: the first section describes the general phenomenological model for the coherent PGE and the experimental validation of the photo-induced sum-frequency process. The second section focuses on the development of the equations governing the dynamic formation of the space-charge grating for SHG process and the subsequent extraction of the phase of the process, the photogalvanic coefficient, and photoconductivities in  $\text{Si}_3\text{N}_4$ . The last section relates these extracted material parameters to the achievable SHG efficiencies of a given platform.

## 2. Photoinduced Generation of Coherent Currents in Centrosymmetric Media

### 2.1. Phenomenological Model

In this section, we analyze the movement of a trapped charge carrier that is exposed to coherently related fields yielding multiphoton absorption interference. We start by defining our model in which under an unperturbed Hamiltonian  $\mathbb{H}_0$  the charge carrier is trapped in state  $|\Psi_g(t)\rangle$  and can be excited to the conduction band  $|\Psi_e(t)\rangle$  via absorption of coherently related photons with optical wavevectors of  $k_1$ ,  $k_2$ , and  $k_3$  and angular frequencies  $\omega_1$ ,  $\omega_2$ , and  $\omega_3$  satisfying  $\omega_3 = \omega_1 + \omega_2$ , as shown in Figure 1. Here  $|\Psi_n(t)\rangle = |n\rangle e^{-i\omega_n t}$  ( $n = \{g, e\}$ ). The charge carrier excitation to conduction band by optical fields enables currents inside the

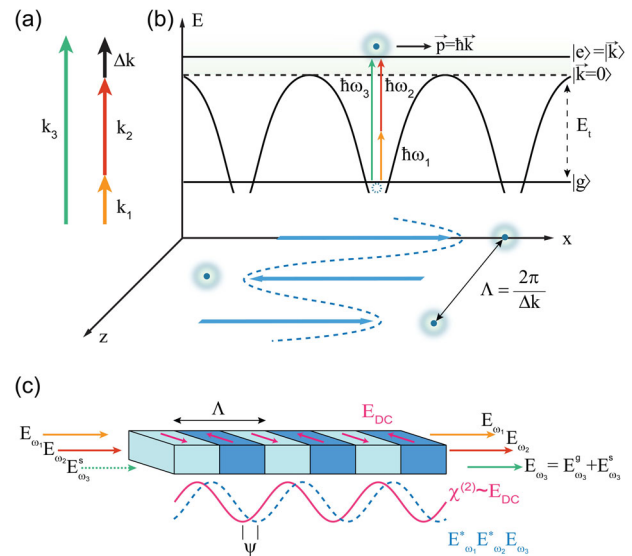


**Figure 1.** a) The phase matching diagram for SFG QPM gratings. b) Charge transport mechanism in AOP for SFG. The directional movement of charges ( $\vec{p} = \hbar \vec{k}$ ) are due to the interference of one photon (angular frequency  $\omega_3$ , wavevector  $k_3$ ) and two photons (frequency  $\omega_1$  and  $\omega_2$ , wavevectors  $k_1$  and  $k_2$ ) ionization pathways from trap  $|g\rangle$  with  $E_t$  being the depth of the trap to excited state  $|e\rangle$ . The movement is periodic along the propagation direction and is dependent on the wavevectors mismatch  $\Delta k = k_3 - k_1 - k_2$  of incident waves resulting in a space-charge field with period  $\Lambda$ . c) The schematic of optically inscribed QPM gratings with period  $\Lambda$  is shown. There can be a phase shift  $\psi$  between the inscribed  $\chi^{(2)}$  grating and the product of the participating fields.

material. We assume the interacting field as phase-locked, and its vector potential,  $\vec{\mathcal{A}}$ , stated as

$$\vec{\mathcal{A}} = \sum_{j=1}^3 \vec{\mathcal{A}}_{\omega_j} e^{i(k_j z - \omega_j t)} + \text{c.c.} \quad (1)$$

where  $k_j$  ( $j = \{1, 2, 3\}$ ) are wavevectors of the absorbed photons, and *c.c.* stands for complex conjugate. In the model we will assume that the light fields are polarized along the *x*-direction while propagating along *z*-axis. It is important to note that, as shown in the energy diagram in Figure 1, the charge carrier can be excited with a single photon at  $\omega_3$ , while it requires two photons with lower energy,  $\omega_1$  and  $\omega_2$ , respectively, for ionization of the same charge carrier. Because the traps are deep ( $E_t/kT \gg 1$ ), it is assumed all carriers are initially in the trap ( $a_e^{(0)} = 0$ ). When a carrier in the trap state is subject to light, the interaction potential in the long wavelength limit is  $\mathbb{V} = -\frac{q}{m} \vec{\mathcal{A}} \cdot \vec{p}$ , where  $q$ ,  $m$ , and  $\vec{p}$  are the charge, mass, and momentum operator, respectively. We are interested in the one dimensional problem so we will drop the vector signs in the potential. The coefficients for single photon absorption ( $a_e^{(1)}$ ) of the sum-frequency (SF) photon of frequency  $\omega_3 = \omega_1 + \omega_2$  and two photon absorption ( $a_e^{(2)}$ ) of frequencies  $\omega_1$  and  $\omega_2$  are acquired using first- and second-order perturbation theory, respectively. Then the probability amplitude of the excited state is  $a_e \approx a_e^{(0)} + a_e^{(1)} + a_e^{(2)}$  and is proportional to<sup>[39]</sup>

$$a_e \sim p_{eg} \mathcal{A}_{\omega_3} + \gamma p_{ei} p_{ig} \mathcal{A}_{\omega_1} \mathcal{A}_{\omega_2} \quad (2)$$

where  $\gamma$  is constant, the momentum holds the relation  $p_{ab} = \langle a | p | b \rangle$ ,  $|i\rangle$  is the intermediate state. The momentum has an odd parity in position, and the charge density that is related to  $|a_e|^2$  normally contains even powers of momentum (or  $k$ ). Therefore, under absorption, the charge density change does not give rise to a directional current. However, it becomes uneven in momentum space when the power of  $k$  is uneven in the cross terms of  $|a_e|^2$ .<sup>[4,12]</sup> This leads to an asymmetry in ionization due to interference of one- and two-photon dipole moments.<sup>[3]</sup> Using that the electric field  $E = -\frac{\partial A}{\partial t}$ , that is,  $E_{\omega_j} = i\omega_j A_{\omega_j}$ , the ionization rates parallel ( $\dot{\rho}^+$ ) and anti-parallel ( $\dot{\rho}^-$ ) to the vector potential become  $\dot{\rho}^\pm \approx |E_{\omega_3} \pm i\zeta E_{\omega_1} E_{\omega_2}|^2$ , where  $E_{\omega_i}$  is the electric field amplitude of light of frequency  $\omega_i$ , and  $\zeta$  is a constant linked to the ionized charge's momentum and absorption cross-sections.

Such anisotropic excitation leads to a photocurrent  $j_{ph} \sim \dot{\rho}^+ - \dot{\rho}^-$ . Including the higher-order perturbations from deeper traps, we can write the photocurrent as  $j_{ph} = (\beta_0 + \beta_{100}|E_{\omega_1}|^2 + \beta_{010}|E_{\omega_2}|^2 + \beta_{001}|E_{\omega_3}|^2 + \dots)E_{\omega_3}E_{\omega_1}^*E_{\omega_2}^*e^{i\Delta k z}e^{-i\psi} + c.c.$ , where  $\psi$  is the phase shift between the inscribed grating and the product of the participating fields ( $E_{\omega_3}E_{\omega_1}^*E_{\omega_2}^*$ ) at any given point in the waveguide (Figure 1b), and  $\beta_{ijk}$  is the photogalvanic coefficient found from  $(i+j+k+2)^{th}$  perturbation,  $\Delta k = k_3 - k_1 - k_2$  is the unmatched wavevectors of absorbed photons. As described in Figure 1b, the contributing light at  $\omega_3$  consists of both the seed ( $E_{\omega_3}^s$ ) and the generated wave from the inscribed grating ( $E_{\omega_3}^g$ ). The excitation of charge carriers also leads to increase in conductivity  $\sigma = \sigma_{001}I_{\omega_3} + \sigma_{110}I_{\omega_1}I_{\omega_2} + \sigma_{101}I_{\omega_1}I_{\omega_3} + \sigma_{011}I_{\omega_2}I_{\omega_3} + \sigma_{002}I_{\omega_3}^2 + \dots$ , where  $I_{\omega_i}$  is the intensity of light of frequency  $\omega_i$  and  $\sigma_{ijk}$  is the photoconductivity coefficient of  $i+j+k$  photon absorption where the subscript denotes the number of photons absorbed having frequencies  $\omega_1, \omega_2$ , and  $\omega_3$ , respectively. Considering only the second-order perturbation, we can simplify the expressions for the induced photocurrent and conductivity as Equations (3) and (4), respectively

$$j_{ph} = \beta E_{\omega_3} E_{\omega_1}^* E_{\omega_2}^* e^{i\Delta k z} e^{-i\psi} + c.c. \quad (3)$$

$$\sigma = \sigma_{001}I_{\omega_3} + \sigma_{110}I_{\omega_1}I_{\omega_2} \quad (4)$$

As can be seen both the anisotropic current and conductivity depend nonlinearly on the optical fields and intensities. In a final steady state, the charge separation leads to the inscription of a static electric field  $E_{DC}$

$$E_{DC} = -\frac{j_{ph}}{\sigma} \quad (5)$$

where the sign of the current is spatially modulated in the  $x$ - $z$  plane (Figure 1) along the light propagation direction due to unmatched wavevector  $\Delta k$  of absorbed photons. The momentum mismatch leads to the spatial modulation of DC field with a period  $\Lambda = 2\pi/\Delta k$ .

## 2.2. Experimental Validation

While our general model predicts the existence of SFG QPM gratings, all coherent PGE demonstrations so far were for the degenerate SHG case, where  $\omega_1 = \omega_2 = \omega_3/2$ . To validate our model we

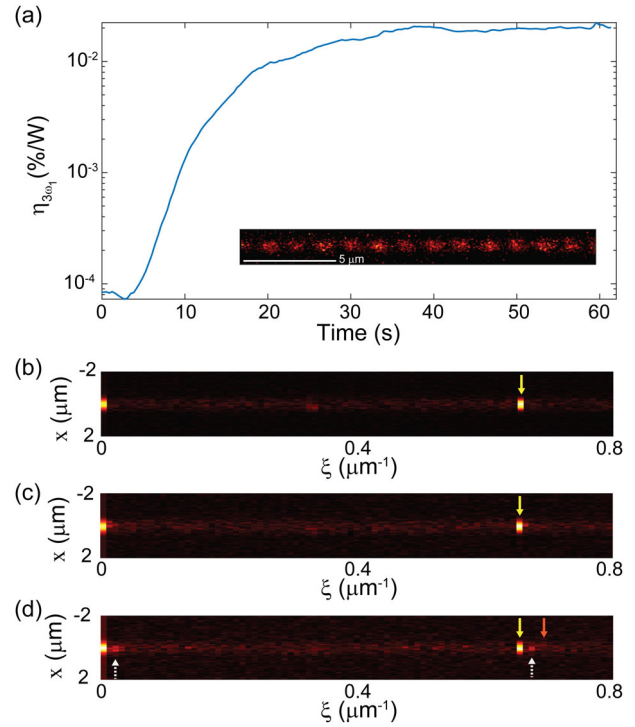


**Figure 2.** a) Growth of TH (SF) conversion-efficiency during AOP with the introduction of pump and its externally generated SH in time. The average outcoupled pump power is 43.6 mW while the SH is 0.3 mW. Inset: TPM image of the first meander of the waveguide. Spatially-resolved Fourier analysis of TPM images of  $\chi^{(2)}$  gratings in b) first, c) sixth, and d) ninth meander of 9 cm long waveguide folded in nine meanders with cross-section of  $0.57 \mu\text{m} \times 0.81 \mu\text{m}$  with  $75 \mu\text{m}$  bend radii as described in ref. [22]. The yellow arrow identifies the primary grating for SHG, the orange arrow—the secondary grating for SFG, and the dashed white arrows—the interference between the two.

used the experimental setup described in Section S1, Supporting Information: a  $1.55 \mu\text{m}$  pump ( $\omega_1$ ) and its SH ( $\omega_2 = 2\omega_1$ ), shaped in ns pulses, are simultaneously coupled to a 9 cm long  $\text{Si}_3\text{N}_4$  waveguide folded in meanders and with  $0.57 \mu\text{m} \times 0.81 \mu\text{m}$  cross-section. It was previously observed<sup>[33]</sup> that coupling only the pump light results in the spontaneous growth of its SH power at the output of waveguide. However, when both pump and its SH are coupled, in addition to a SHG, we can also clearly observe the spontaneous growth of third-harmonic generation (THG) ( $3\omega_1$ ) due to a cascaded second-order process. The measured growth of THG conversion efficiency (CE) defined as  $\eta_{3\omega_1} = P_{3\omega_1}/(P_{2\omega_1}P_{\omega_1})$  is shown in Figure 2. As the grating period is related to the wavevector mismatch of the participating optical waves, those can be revealed from processing the grating images captured by TPM imaging.<sup>[24]</sup> Such an image can be seen in the inset of Figure 2a. In order to precisely retrieve the grating components, we perform a spatially resolved Fourier analysis on grating images recorded at different positions along the waveguide length. The results for gratings on the first, sixth, and ninth meanders are shown in Figure 2b–d, respectively.

We see in the first meanders a single non-zero spatial frequency (yellow arrow) which corresponds to the grating phase-matched to the interference of pump-SH absorption, having

wavevector mismatch of  $\Delta k_1 = k_{2\omega_1} - 2k_{\omega_1}$ . In the last meander, additional non-zero spatial frequencies appear owing to the inscription of a secondary grating due to the interference of pump-SH-TH absorption, assumed to have wavevector mismatch of  $\Delta k_2 = k_{3\omega_1} - k_{\omega_1} - k_{2\omega_1}$  (orange arrow). Considering that the final  $\chi^{(2)}$  grating is composed of two parts, the measured  $(\chi^{(2)})^2$  response should possess four non-zero spatial frequencies proportional to  $2|\Delta k_1|$ ,  $2|\Delta k_2|$ , and interference terms  $|\Delta k_1 + \Delta k_2|$  and  $|\Delta k_1 - \Delta k_2|$ . In our case, the secondary grating being weak, its spatial frequency does not clearly appear but can still be easily retrieved based on the interference terms (dashed white arrows). A narrow waveguide, supporting only the fundamental TE mode at the pump wavelength, is used for the experimental validation as to reduce the number of possible interactions for a more precise quantification. The experimentally obtained spatial frequency related to  $2|\Delta k_1|$  and inferred  $2|\Delta k_2|$  are in agreement within 3% errors with those obtained from finite element method simulations, considering pump-SH and pump-SH-TH photogalvanic processes involving dominantly fundamental mode interactions. Here, the pump-SH-TH photogalvanic process occurs spontaneously. The grating appears at the end of the waveguide similar to what has been observed using TPM imaging and spectral bandwidth measurements in case of spontaneous AOP for SHG.<sup>[21,22,33,40]</sup> This demonstration unambiguously confirms the plausibility of AOP for SFG process, as exposed in our generalized model, and could be extended to any three coherently related input waves.

### 3. Time Dynamics of All-Optical Poling and Its Dependence on Waveguide Modes

#### 3.1. Theoretical Bases

In this section, we present the governing equation for the formation of space-charge gratings under coherently related fields, focusing on the SHG enabled by coherent PGE. In this case, we denote the pump frequency as  $\omega_1$  and thus the seeded SH is at frequency of  $2\omega_1$ . We can rewrite Equation (3) as  $j_{ph} = \beta E_{2\omega_1} (E_{\omega_1}^*)^2 e^{i\Delta k_1 z} e^{-i\psi}$  and Equation (4) as  $\sigma = \sum_{a,b} \sigma_{ab} I_{\omega_1}^a I_{2\omega_1}^b$  for  $a \geq 2$  and  $b \geq 0$ , where  $\beta$  is a function of intensities of pump and SH due to the contributions of higher-order perturbations or involvement of other states, that is,  $\beta = \sum_{a,b} \beta_{ab} I_{\omega_1}^a I_{2\omega_1}^b$ .<sup>[41]</sup> We start by solving the continuity equation and Maxwell's equations together under slowly-varying envelope and undepleted pump approximation<sup>[13]</sup> (see Section S2, Supporting Information). Introducing the walk-off between the pump and SH with a term  $g(z) = e^{-(z/L_w)^2}$ , where  $L_w$  the temporal walk-off length is a function of group-velocity mismatch of involved modes (see Section S3, Supporting Information), as  $|E_{\omega_1}| \rightarrow |E_{\omega_1}|g(z)$ ,<sup>[17]</sup> we obtain

$$\frac{\partial^2 \bar{E}}{\partial t \partial z} - \frac{3\omega_1 \chi^{(3)}}{2n_{2\omega_1} c \epsilon} \beta |E_{\omega_1}|^4 e^{i(\frac{z}{L_w} - \psi)} g^4(z) \bar{E} = 0 \quad (6)$$

where  $\bar{E} = E_{2\omega_1} e^{i/\tau} e^{\alpha z/2}$  with the decay time  $\tau = \epsilon/\sigma$ ,  $\epsilon$  being the dielectric constant of the material, and  $\alpha$  is the propagation loss coefficient of SH.

The optical modes participating in the grating inscription should also be examined. We use the separability of the modes in different dimensions, that is,  $E_{q\omega_1}^{(w)}(\vec{r}, t) = U_{q\omega_1}^{(w)}(x, y) A_{q\omega_1}^{(w)}(z, t)$  ( $q = 1, 2$ ), where  $U_{q\omega_1}^{(w)}$  describes the normalized transverse field and  $A_{q\omega_1}^{(w)}$  is the field amplitude along the  $z$ -axis of the  $w^{\text{th}}$  mode. In addition, we multiply both sides of the Equation (6) with  $\iint dx dy (U_{2\omega_1}^{(w)}(x, y))^*$  and define normalization  $\iint dx dy |U_{q\omega_1}^{(w)}(x, y)|^2 = 1$  to obtain

$$\frac{\partial^2 A^{(l)}}{\partial t \partial z} = M_p \Gamma_{pl} A^{(l)} - \sum_{a,b} \frac{e^{-\alpha z} |A_{\omega_1}^{(p)}|^{2a} |A^{(l)}|^{2b}}{\tau_{ab}^{\text{eff}} (S_{\omega_1}^{(p)})^a (S_{2\omega_1}^{(l)})^b} \frac{\partial A^{(l)}}{\partial z} \quad (7)$$

where  $M_p = \frac{i3\omega_1 \chi^{(3)}}{2n_{2\omega_1} c \epsilon} \beta |A_{\omega_1}^{(p)}|^4 e^{-i\psi}$ ,  $S_{\omega_1}^{(p)}$  and  $S_{2\omega_1}^{(l)}$  are the effective areas of pump and SH modes as defined in Section S4, Supporting Information.  $\tau_{ab}^{\text{eff}} = \frac{\epsilon}{\sigma_{ab} \kappa_{ab}} \frac{2^{a+b}}{(\epsilon_0 c)^{a+b} n_{2\omega_1}^a n_{\omega_1}^b}$ ,  $\kappa_{ab} = S_{\omega_1}^{(p)a} S_{2\omega_1}^{(l)b} \iint dx dy |U_{\omega_1}^{(p)}(x, y)|^{2a} |U_{2\omega_1}^{(l)}(x, y)|^{2b+2}$ ,  $A^{(l)} = A_{2\omega_1}^{(l)} e^{\alpha z/2}$  and we define the overlap integral of modes for  $C_{4v}$  point group as

$$\Gamma_{pl} = \iint dx dy |U_{\omega_1}^{(p)}(x, y)|^4 |U_{2\omega_1}^{(l)}(x, y)|^2 \quad (8)$$

where the symmetries of third-order susceptibility and nonlinear conductivity are hidden here. It describes the effective nonlinear overlap of the modes (unit of  $m^{-4}$ ) in the grating writing and SH generation process. Here,  $A^{(l)}$  is independent of area of the waveguide as the power transferred in the mode  $l$  is  $\frac{n_{2\omega_1} c \epsilon_0}{2} |A_{2\omega_1}^{(l)}|^2$ . The information on the waveguide dimensions is hidden in the overlap integral. The overlap integral is in the same order of magnitude for different modes and can be simulated numerically (see Section S2, Supporting Information). Hence, the inscription of QPM gratings of different modes is allowed as observed in other works.<sup>[24,42]</sup> The same applies to the more generalized SFG process.

As evident, the governing Equation (6) encloses important material constants that should be addressed in order to quantify the capabilities of a given platform:  $\beta$  will determine the magnitude of the coherent photocurrent, which will be counterbalanced by the increase in conductivity  $\sigma$  owing to the excitation of charge carriers. Another important term in the Equation (6) is the phase shift  $\psi$  between the inscribed grating and product of participating optical fields. In most analyses of the coherent PGE in optical waveguides, it is assumed to be  $\pi/2$ , which is justified by the fact that coherent current is caused by the  $\pi/2$  phase difference in the single and two-photon ionizations.<sup>[8,43]</sup> However, the phase of the photocurrent can be different if the influence of the atomic potential is considered.<sup>[8,44,45]</sup> In the following subsections we experimentally extract  $\beta$ ,  $\sigma$ , and  $\psi$  that will provide means for quantitative assessment of the capabilities of  $\text{Si}_3\text{N}_4$  platform for SHG.

#### 3.2. Experimental Extraction of $\psi$ , $\beta$ , and $\sigma$ in $\text{Si}_3\text{N}_4$ Waveguides

Parametric optical and photogalvanic processes can have different phase shifts.<sup>[8,35,44,45]</sup> In ref. [19], the steady state phase of the generated SH with respect to the seed SH was measured to be  $\pi/2$  for silica fibers. From that, it was concluded the phase of



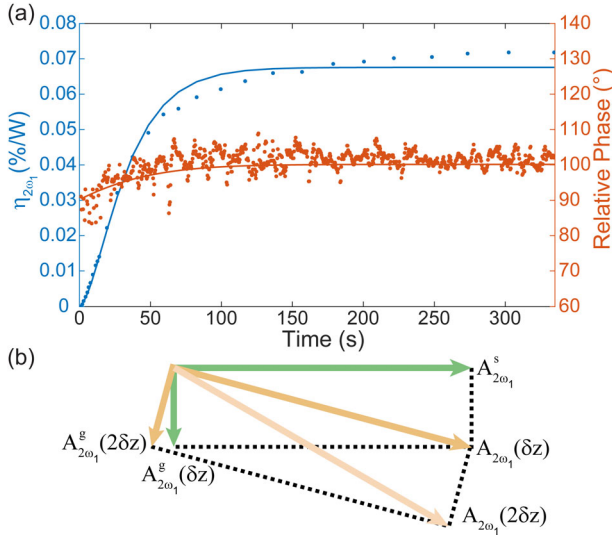


**Figure 3.** a) CE and relative phase of the generated SH with respect to the seed phase during AOP. Dots are experimental data and lines are fits. The CE was fitted using Equation (9b) for  $\psi = 0$ . b) Evolution of the total SH amplitude ( $A_{2\omega_1}$ ) and phase along the waveguide for  $\psi = 0$ . Arrows represent the fields and their phases and different colors represent different positions. At position 0, the seed  $A_{2\omega_1}^s$  having 0 phase is injected. Along with the generated field  $A_{2\omega_1}^g(\delta z)$  they contribute to the total field  $A_{2\omega_1}^s(\delta z)$ . The total field becomes the inscribing field for that position and generates  $A_{2\omega_1}^g(2\delta z)$  at position  $2\delta z$ .

inscribed  $\chi^{(2)}$  grating is the same as the product of the participating fields  $(E_{\omega_1}^*)^2 E_{2\omega_1}$ , that is,  $\psi = 0$ . In order to extract the dynamic phase of the grating for the  $\text{Si}_3\text{N}_4$  waveguide, we seed the AOP process and measure the interference between the seed and the generated SH. We use a 43 mm long waveguide with  $1.5 \mu\text{m} \times 0.8 \mu\text{m}$  cross-section, and inject pump and SH with peak powers of 8.57 W and 400 mW, respectively. Without the loss of generality, we consider the field amplitude of SH seed at the input of the waveguide writes as  $A_{2\omega_1}^s$  with an initial phase of 0, the generated SH field amplitude is of the form  $A_{2\omega_1}^g e^{i\varphi}$ . If we consider the process at the beginning of the waveguide, the input SH seed ( $A_{2\omega_1}^s$ ) leads to generated SH  $A_{2\omega_1}^g(\delta z)$  after a distance  $\delta z$ . Clearly, if the SH generated is strong enough to contribute to the subsequent grating inscription, that is,  $A_{2\omega_1}^s + [A_{2\omega_1}^g(\delta z)]$  becomes the new seed, this grating will be shifted by a phase related to the strength of  $A_{2\omega_1}^g(\delta z)$ . The same then occurs throughout the length of the waveguide and it is expected that the grating will thus have a varying phase. This is illustrated in **Figure 3b**, for the specific case of  $\psi = 0$ . As Equation (6) is symmetric in position and time, analogous evolution of fields happen in time as well. In the case of high seed power, the grating inscription is dominated by the seed SH such that the contribution of the internally generated SH can be considered negligible. Under this limit, we can minimize the phase evolution and extract  $\psi$  from the generated SH phase by measuring the initial phase  $\varphi(t \ll \tau) \approx \pi/2 - \psi$ . The CE is defined as  $\eta_{2\omega_1} = P_{2\omega_1}/P_{\omega_1}^2 = \frac{2n_{2\omega_1}|A_{2\omega_1}^g|^2}{\epsilon_0 c n_{\omega_1}^2 |A_{\omega_1}|^4}$  and experimentally retrieved phase  $\varphi$  during the poling process are shown in **Figure 3**. In **Figure 3a**, we show the experimen-

tal data and theoretical fit which are in good agreement. Small discrepancies are observed around the saturation region, which could come from small variations in the poling conditions with time. Out of 90 poling events in four different waveguides, we extract  $\psi = -1.9^\circ \pm 14.8^\circ$  (or similarly  $181.9^\circ \pm 14.8^\circ$ ). We attribute the fluctuations to the weak generated SH in the beginning of the process reducing the resolution of the interference measurements. Similar to ref. [19], we can conclude that the total generated SH and the inscribed grating are in phase, that is,  $\psi = 0$  in our case.

We extract the material parameters  $\beta$  and  $\sigma$  through a series of experiments. To link results to theory, we make certain assumptions and design the experiments accordingly. We first assume that the dark conductivity is very small compared to the photoconductivity.<sup>[22,46,47]</sup> Therefore, we can ignore the grating erasure due to dark conductivity. In order to linearize the equation, we assume the pump and SH powers are constant except for the linear losses. This assumption can be justified once again in the case of high seed power since it will dominate the total SH in the poled waveguide. Using such approximations we solve Equation (6) (see Section S2, Supporting Information), to get the second-order susceptibility and SH field. For the generalized case of a constant pump and seed in the  $p^{\text{th}}$  and  $l^{\text{th}}$  modes, respectively, the solution is expressed as

$$\chi_{pl}^{(2)}(\vec{r}, t) = \frac{3\chi^{(3)}}{\epsilon} \beta \left( E_{\omega_1}^{(p)*}(x, y) \right)^2 E_{2\omega_1}^{(s,l)}(x, y) e^{i(\Delta k_1 z - \psi)} g^2(z) e^{-\alpha z/2} \int_0^t dt' J_0(2\sqrt{-M_p \Gamma_{pl} G(z)t'}) e^{-t'/\tau} + \text{c.c.}, \quad (9a)$$

$$A_{2\omega_1}^{g,l}(z, t) = -A_{2\omega_1}^{s,l} e^{-\alpha z/2} \int_0^{2\sqrt{-M_p \Gamma_{pl} G(z)t}} d\xi e^{\xi^2/4M_p \Gamma_{pl} G(z)\tau} J_1(\xi) \quad (9b)$$

It can be seen that the  $\chi^{(2)}$  grating adjusts its shape to the product of involved modes, that is,  $(E_{\omega_1}^*)^2 E_{2\omega_1}$  and is periodic with a period  $\Lambda = 2\pi/\Delta k_1$ . Under this configuration,  $\beta$  and  $\sigma$  can be extracted by fitting the time dynamics of the SHG CE with Equation (9b). We also assume that the process occurs dominantly on fundamental modes for both pump and SH, as previously shown. Hence, for the remainder of the paper we will not denote the mode number in overlap integrals and amplitudes. The optical setup and procedures for the measurements are described in Section S1, Supporting Information.

Equation (9b) accounts for the waveguide cross-section and coupled light power, hence, according to the theory, the calculated photogalvanic coefficient and conductivity should not depend on the waveguide cross-section. After extracting the phase of the effect, both the cross-sections and powers are swept. Thus, we carried out AOP on four 43 mm long waveguides with different cross-sections (1.1, 1.3, 1.4,  $1.5 \mu\text{m} \times 0.8 \mu\text{m}$ ), and for various coupled pump and coupled SH seed powers. In these waveguides, the nondegenerate SFG (TH) is found to be negligible as they are shorter. The extracted CE data is then fitted using Equation (9b) and examples of the experimental data and fit for the  $1.5 \mu\text{m} \times 0.8 \mu\text{m}$  cross-section waveguide are shown in **Figure 4**. The fits are done by varying parameters  $M_p$  and  $\tau$  for a given seed SH and the simulated overlap integrals are given in Section S4, Supporting Information. From extracted  $M_p$  and  $\tau$ , using

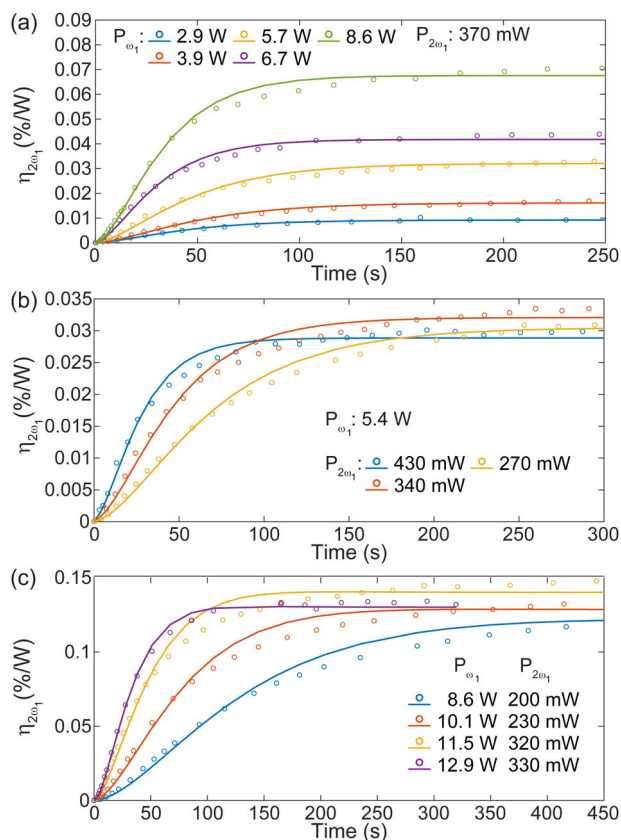


**Figure 4.** Experimental SHG CE during AOP (dotted line) and fit using Equation (9b) (solid line) for a) constant peak SH seed power of 66.2 mW and varying peak pump power; b) constant peak pump power of 3.4 W and varying peak SH seed power; c) varying peak power for both pump and SH seed.

the measured pump power and material parameters given in Section S5, Supporting Information,  $\beta$  and  $\sigma$  are extracted. We can point out that the power requirement to initiate AOP is significantly reduced with seeding compared to the spontaneous process (i.e., only pump is injected in the waveguide).<sup>[22]</sup> We can see in Figure 4a that the initial growth rate and efficiency of the process increases with pump power. When the pump power is fixed and we vary the seed SH power a similar behavior is observed in terms of speed, however, the reached efficiency does not significantly vary, but seems to start decreasing with the highest seed power as shown in Figure 4b. As the photocurrent depends on the  $(A_{\omega_1}^2)^* A_{2\omega_1}$ , the initial growth rate increases with the increase of the product of the coupled power ( $P_{\omega_1}^2 P_{2\omega_1}$ ) but the efficiency is limited as the photoconductivity increases. This is demonstrated in Figure 4c. One can see that similar efficiencies can be reached for lower pump and SH.

The photogalvanic coefficient and photoconductivity can be intensity dependent due to the higher-order perturbations or contribution of deeper states. Higher-order perturbations become prominent either if the deep traps are excited through multiphoton absorption of SH, or via incoherent contributions with intermediate states being involved. Hence, using the data from 90 experimental poling events of the four waveguides, we fit  $\beta$  and  $\sigma$

**Table 1.** Extracted photoconductivity and photogalvanic coefficients.

$\sigma_{10} [\text{S} \mu\text{m} \text{W}^{-1}]$	$\sigma_{01} [\text{S} \mu\text{m} \text{W}^{-1}]$	$\sigma_{02} [\text{S} \mu\text{m}^3 \text{W}^{-2}]$	$\sigma_{21} [\text{S} \mu\text{m}^5 \text{W}^{-5}]$
$\approx 0$	$\approx 0$	$1.19 \times 10^{-15}$	$1.36 \times 10^{-18}$
$\beta_0 [\text{A} \mu\text{m} \text{V}^{-3}]$	$\beta_{10} [\mu\text{m}^3 \text{V}^{-4}]$	$\beta_{01} [\mu\text{m}^3 \text{V}^{-4}]$	$\beta_{20} [\mu\text{m}^5 \text{V}^{-5} \text{A}^{-1}]$
$\approx 0$	$\approx 0$	$8.22 \times 10^{-20}$	$6.17 \times 10^{-23}$

with a polynomial as a function of coupled pump and SH intensities. The fits, presented in Table 1, were obtained using least absolute residuals method with  $R^2 = 0.92$  and  $R^2 = 0.93$ , for  $\beta$  and  $\sigma$ , respectively. The extracted conductivity is orders of magnitude higher than the dark conductivity values found in literature.<sup>[46]</sup> The analysis above allows for the extraction of parameters for photogalvanic effect and can be readily used for characterizing other platforms or the same platform under different fabrication processes. Thus different materials or recipes may be compared in the context of application of AOP via the photogalvanic effect. Nevertheless, further studies linking extracted parameters and microscopic properties of the material are still required.

The fact that our experimental data yields  $\sigma_{01}$  close to zero suggest that the charge carrier is not directly excited from trap state to the conduction band via absorption of a single SH photon. Instead intermediate states are involved or, alternatively, higher-order of the coherent PGE is taking place in the AOP process. In order to gain insight on this, we modified the experimental setup to check if the higher-order contributions to current and conductivity come from higher-order coherent PGE<sup>[10]</sup> or from incoherent photo-excitation from deeper traps working as a carrier source.<sup>[41]</sup> To that end, we split the pump beam and send part of the pump beam backward (probe) in addition to the forward propagating pump and its SH (see Figure S1, Supporting Information) inside a waveguide having cross-section  $1.79 \mu\text{m} \times 0.8 \mu\text{m}$ . We ensured that forward and backward pump and probe pulses are coincidental. The forward propagating pump and SH beams work as coherent sources and the backward propagating beam as the incoherent source. In Figure 5, we sweep the incoherent pump power keeping the coherent sources constant, similar to the work in ref. [41], and observe the increase of the initial speed of the process with increase of incoherent counter-propagating pump power. We extract  $\beta$  by making a parabolic fit to the power using the Taylor approximation of Equation (9b). The increase in  $\beta$  as a function of backward propagating probe, and hence increase in the photocurrent from the forward propagating pump and SH, is an evidence of deeper traps working as a charge carrier source. The backward probe promotes carriers to intermediate state, thus increasing the number of carriers which can then be involved in the third-order coherent PGE as shown in Figure 1. While higher-order coherent PGEs may also explain such behavior, as pointed out in ref. [41], such effects are much less probable. Our observations are therefore in agreement with the three-photon model and involvement of intermediate states.

#### 4. Conversion Efficiency and Performance Limitations

The measured material parameters now provide means for making a quantitative study of achievable SHG CE in the  $\text{Si}_3\text{N}_4$

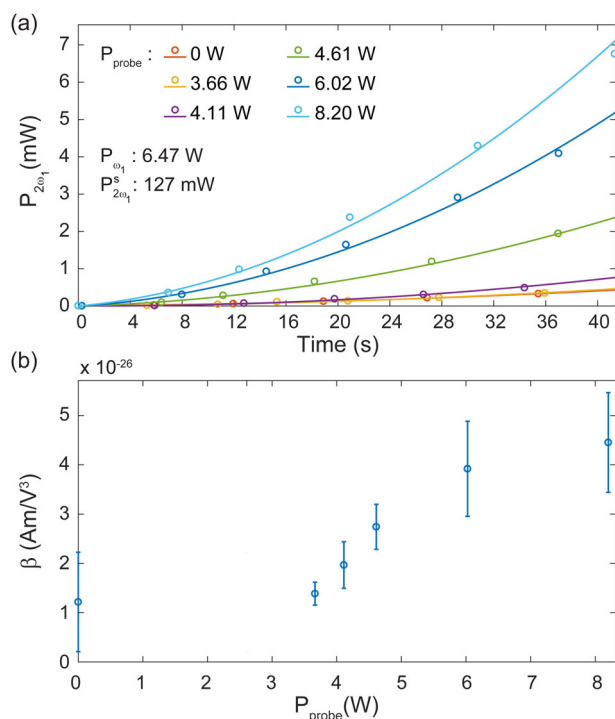


**Figure 5.** a) Generated SH power as a function of time for the probe light of varying peak powers. During the different poling events, the forward propagating pump and SH powers are kept constant. Dots are experimental data, lines are fits. The waveguide has a cross section of  $1.79 \times 0.8 \mu\text{m}^2$ . b) Extracted  $\beta$  from fit as a function of probe power.

platform. It is important to emphasize, that due to the phase parameter  $\psi$  which in our case is 0, the output generated SH and the input seed SH may have a phase difference as illustrated in Figure 3b. The phase variation depends on waveguide length, initial SH seed power as well as SH power generated inside the waveguide, and it is expected that the grating will thus have a varying phase.

By analytically solving the governing Equation (6) in a steady state, we obtain the amplitude and phase of SH generated inside the waveguide after AOP (see Equations (S22) and (S23), Supporting Information). The simulated relative amplitude and phase of

the generated SH as a function of seed amplitude and waveguide length are plotted in Figure 6a,b, respectively. For high seed powers, the grating inscription is dominated by the seed field and the phase change is relatively slow along the length. For low seed powers where generated light power is comparable with the seed light power, the grating inscription is influenced by both the seed and the generated field. There are oscillations in the phase and generated field amplitude along the length. As the seed power reduces, the phase and efficiency fluctuations become more pronounced. This is due to the one part of the grating that is interfering destructively with another part of the grating, since  $\psi$  is not equal to  $\pm\pi/2$  as considered earlier. Hence, the oscillations of simulated SH power and phase as shown in Figure 6a,b are solely due to  $\psi$  being equal zero. Another limiting factor comes from the increase of the photoconductivity with increased seed power. For high seed powers, conductivity takes over the photocurrent and the effective  $\chi^{(2)}$  reduces, as seen from Equation (5). However, as the phase change is small the achievable CE rises with the length for high seed powers where grating inscription is dominated by the seed light. From the simulations, it is observed that the achievable CE rises over 1.4 %/W for a 20 cm long waveguide at seed power of 3 mW. The evident trend of CE growth suggests that the efficiency can be further increased using even longer waveguides and higher seed powers.

## 5. Conclusions

In this work, we extend the phenomenological model proposed by Dianov et al.<sup>[13]</sup> to understand the underlying physics and dynamics of the AOP process in waveguides, and to develop physical bases to compare different photonic material platforms. We observe the dynamic phase for SHG process in  $\text{Si}_3\text{N}_4$  and extract the phase shift ( $\psi$ ) between the inscribed grating and the product of the participating fields to be approximately 0 or  $\pi$ . For the first time, we find a solution for the governing equation at high seed approximation and, therefore, we retrieve the photogalvanic coefficient  $\beta$  and photoconductivity  $\sigma$  for  $\text{Si}_3\text{N}_4$ , and make predictions of the expected efficiencies. It is shown that that by using optical seeding, the energy requirements for achieving AOP can be reduced by an order of magnitude, while the speed increased drastically compared to the spontaneous AOP. In addition, we

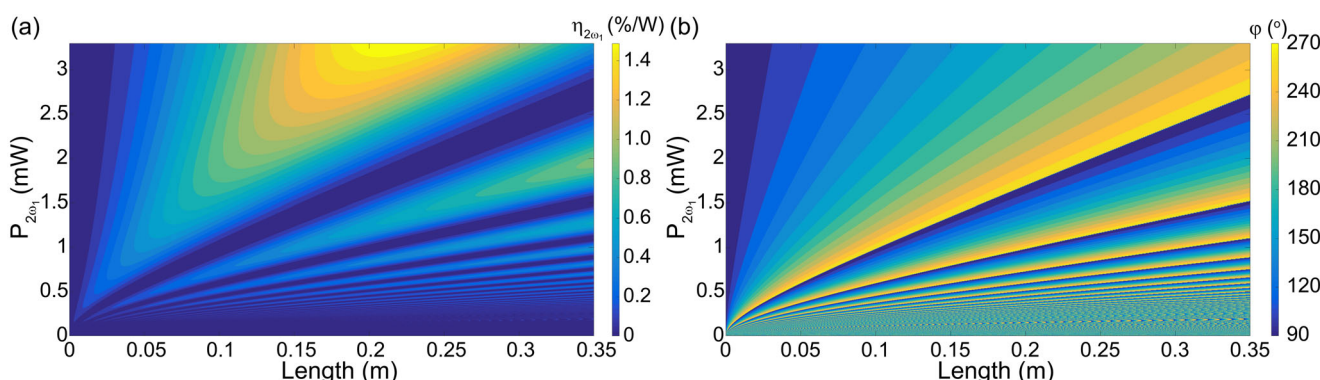


**Figure 6.** a) Estimated CE (%/W) for a waveguide of cross-section  $1.4 \mu\text{m} \times 0.8 \mu\text{m}$  and b) phase of the generated SH ( $\phi$ ) along the length and average seed power is shown for  $\psi = 0$ . Simulation is done for the material constants in Table 1 and average pump power of 0.1 W. For a certain length, the maximum conversion efficiency can be optimized with the introduction of external seed power.



predict and provide the first experimental demonstration of the inscription of  $\chi^{(2)}$  gratings for the general case of SF generation.

## Supporting Information

Supporting Information is available from the Wiley Online Library or from the author.

## Acknowledgements

This work was supported by ERC grant PISSARRO (ERC-2017-CoG 771647). The samples used for the experiment were fabricated by LIGEN-TEC SA.

Open access funding provided by Ecole Polytechnique Federale de Lausanne (EPFL).

## Conflict of Interest

The authors declare no conflict of interest.

## Data Availability Statement

The data that support the findings of this study are available from the corresponding author upon reasonable request.

## Keywords

nonlinear optics, nanophotonics, nonlinear waveguides, photogalvanic effect, second-order nonlinear effects

Received: April 26, 2022

Revised: July 7, 2022

Published online: September 14, 2022

- [1] E. Manykin, A. Afanas'ev, *Sov. Phys. JETP* **1967**, 25, 828.
- [2] D. J. Jackson, J. J. Wynne, P. H. Kes, *Phys. Rev. A* **1983**, 28, 781.
- [3] E. Dupont, P. B. Corkum, H. C. Liu, M. Buchanan, Z. R. Wasilewski, *Phys. Rev. Lett.* **1995**, 74, 3596.
- [4] R. Atanasov, A. Haché, J. L. P. Hughes, H. M. van Driel, J. E. Sipe, *Phys. Rev. Lett.* **1996**, 76, 1703.
- [5] A. Haché, Y. Kostoulas, R. Atanasov, J. L. P. Hughes, J. E. Sipe, H. M. van Driel, *Phys. Rev. Lett.* **1997**, 78, 306.
- [6] W. Pötz, W. A. Schroeder, in: *Proc. of an Int. Workshop held in Chicago*, Vol. 19, Springer, New York **1998**.
- [7] J. Rioux, G. Burkard, J. E. Sipe, *Phys. Rev. B* **2011**, 83, 195406.
- [8] N. B. Baranova, H. R. Reiss, B. Y. Zel'dovich, *Phys. Rev. A* **1993**, 48, 1497.
- [9] E. Baskin, M. Entin, *Sov. J. Exp. Theor. Phys. Lett.* **1988**, 48, 601.
- [10] D. Z. Anderson, V. Mizrahi, J. E. Sipe, *Opt. Lett.* **1991**, 16, 796.
- [11] B. Y. Zel'Dovich, A. Chudinov, *Sov. J. Exp. Theor. Phys.* **1989**, 50, 439.
- [12] N. Baranova, A. Chudinov, B. Y. Zel'dovich, *Opt. Commun.* **1990**, 79, 116.
- [13] E. M. Dianov, P. G. Kazansky, D. Y. Stepanov, *Proc. SPIE* **1991**, 1516, 81.
- [14] U. Österberg, W. Margulis, *Opt. Lett.* **1986**, 11, 516.
- [15] W. Margulis, F. Laurell, B. Lesche, *Nature* **1995**, 378, 699.
- [16] E. M. Dianov, D. S. Starodubov, *Quantum Electron.* **1995**, 25, 395.
- [17] H. W. K. Tom, R. H. Stolen, G. D. Aumiller, W. Pleibel, *Opt. Lett.* **1988**, 13, 512.
- [18] D. M. Krol, J. R. Simpson, *Opt. Lett.* **1991**, 16, 1650.
- [19] W. Margulis, I. C. Carvalho, J. P. von der Weid, *Opt. Lett.* **1989**, 14, 700.
- [20] A. Billat, D. Grassani, M. H. Pfeiffer, S. Kharitonov, T. J. Kippenberg, C.-S. Brès, *Nat. Commun.* **2017**, 8, 1016.
- [21] D. D. Hickstein, D. R. Carlson, H. Mundoor, J. B. Khurgin, K. Srinivasan, D. Westly, A. Kowligy, I. I. Smalyukh, S. A. Diddams, S. B. Papp, *Nat. Photonics* **2019**, 13, 494.
- [22] E. Nitiss, T. Liu, D. Grassani, M. Pfeiffer, T. J. Kippenberg, C.-S. Brès, *ACS Photonics* **2019**, 7, 147.
- [23] X. Lu, G. Moille, A. Rao, D. A. Westly, K. Srinivasan, *Nat. Photonics* **2021**, 15, 131.
- [24] E. Nitiss, J. Hu, A. Stroganov, C.-S. Brès, *Nat. Photonics* **2022**, 16, 134.
- [25] D. J. Blumenthal, R. Heideman, D. Geuzebroek, A. Leinse, C. Roeloffzen, *Proc. IEEE* **2018**, 106, 2209.
- [26] C. J. Krückel, V. Torres-Company, P. A. Andrekson, D. T. Spencer, J. F. Bauters, M. J. Heck, J. E. Bowers, *Opt. Lett.* **2015**, 40, 875.
- [27] A. Ayan, F. Mazeas, J. Liu, T. J. Kippenberg, C.-S. Brès, *Opt. Express* **2022**, 30, 4342.
- [28] J. S. Levy, M. A. Foster, A. L. Gaeta, M. Lipson, *Opt. Express* **2011**, 19, 11415.
- [29] D. Grassani, E. Tagkoudi, H. Guo, C. Herkommer, F. Yang, T. J. Kippenberg, C.-S. Brès, *Nat. Commun.* **2019**, 10, 1553.
- [30] A. L. Gaeta, M. Lipson, T. J. Kippenberg, *Nat. Photonics* **2019**, 13, 158.
- [31] E. Sahin, B. Zabelich, O. Yakar, E. Nitiss, J. Liu, R. N. Wang, T. J. Kippenberg, C.-S. Brès, *Nanophotonics* **2021**, 10, 1923.
- [32] R. Dalidet, F. Mazeas, E. Nitiss, O. Yakar, A. Stroganov, S. Tanzilli, L. Labonté, C.-S. Brès, *Opt. Express* **2022**, 30, 11298.
- [33] E. Nitiss, O. Yakar, A. Stroganov, C.-S. Brès, *Opt. Lett.* **2020**, 45, 1958.
- [34] R. W. Terhune, D. A. Weinberger, *JOSA B* **1987**, 4, 661.
- [35] R. Stolen, in *Nonlinear Waves in Solid State Physics* (Eds: A. D. Boardman, M. Bertolotti, T. Twardowski), NATO Science Series B, Springer New York, NY **1990**, p. 297.
- [36] R. H. Stolen, H. Tom, *Opt. Lett.* **1987**, 12, 585.
- [37] P. Chmela, *Opt. Lett.* **1988**, 13, 669.
- [38] X. Lu, K. Srinivasan, *Phys. Rev. Appl.* **2021**, 16, 014027.
- [39] L. D. Landau, E. M. Lifshitz, *Quantum Mechanics: Non-Relativistic Theory*, Vol. 3, Pergamon Press, Oxford **2013**.
- [40] E. Nitiss, B. Zabelich, O. Yakar, J. Liu, R. N. Wang, T. J. Kippenberg, C.-S. Brès, *Photonics Res.* **2020**, 8, 1475.
- [41] E. Dianov, P. Kazansky, D. Starodubov, *Sov. Lightwave Commun.* **1993**, 3, 247.
- [42] O. Yakar, E. Nitiss, C.-S. Brès, in *Conf. on Lasers and Electro-Optics*, Optica Publishing Group, Washington DC **2021**, p. JTh3A.
- [43] D. Z. Anderson, V. Mizrahi, J. E. Sipe, in *Int. Workshop on Photoinduced Self-Organization Effects in Optical Fiber*, Vol. 1516, International Society for Optics and Photonics, San Diego **1991**, pp. 154–161.
- [44] D. Anderson, N. Baranova, K. Greene, B. Y. Zel'dovich, *Sov. Phys. JETP* **1992**, 75, 210.
- [45] N. Baranova, B. Y. Zel'dovich, *JOSA B* **1991**, 8, 27.
- [46] M. J. Madou, *Fundamentals of Microfabrication: The Science of Miniaturization*, CRC Press, Boca Raton, FL **2018**.
- [47] E. Tuncer, *Solid-State Electron.* **2017**, 134, 46.